# Flow Cell Characterisation: Flow Visualisation, Pressure Drop and Mass Transport at 2D Electrodes in a Rectangular Channel

**Wu, L., L. F. Arenas, J. E. Graves, and F. C. Walsh**



**Original citation:**
Wu, L., et al. "Flow Cell Characterisation: Flow Visualisation, Pressure Drop and Mass Transport at 2D Electrodes in a Rectangular Channel." *Journal of The Electrochemical Society* 167.4 (2020): 043505.
**http://dx.doi.org/**10.1149/1945-7111/ab7b49

ISSN: 0013-4651

Publisher: Electrochemical Society

# Flow Cell Characterisation: Flow Visualisation, Pressure Drop and Mass Transport at 2D Electrodes in a Rectangular Channel

L. Wu[a,*], L. F. Arenas[b,†], J. E. Graves[a], F. C. Walsh[b]

[a] Functional Materials Group, Institute for Future Transport and Cities, Coventry University, Coventry CV1 5FB, United Kingdom.

[b] Electrochemical Engineering Laboratory, Energy Technology Group, Faculty of Engineering and Physical Sciences, University of Southampton, Southampton, SO17 1BJ, United Kingdom.

* Author for correspondence; L. Wu; ac3448@coventry.ac.uk

[†] Present address: Cuernavaca, Mexico.

## Abstract

Aiming to demonstrate the importance and facility of characterising the reaction environment in new commercial laboratory-scale flow cells, fluid flow, pressure drop and space averaged mass transport coefficient were studied in the C-Flow® Lab 5 × 5 cell. A flow-by configuration with smooth, planar electrodes in a rectangular channel was used. Electrolyte mean linear velocities of 2 to 10 cm $s^{-1}$ past the electrode surface and channel Reynolds numbers of 53 to 265 were considered. The effect of a turbulence promoter next to the working electrode was evaluated. Flow distribution was explored by a qualitative flow visualization study, while the relevance of pressure drop was shown by measurements over the flow channel and the whole cell as a function of mean linear velocity. The electrochemical performance was quantified from the limiting current, permitting the determination of the mass transport coefficient at the electrodes over the same range of flow rates. Reactant conversion in the batch recirculation mode and normalised space velocity were predicted from the electrochemical plug flow reactor design equation. Results were compared to well-characterised electrochemical flow reactors found in the literature. The significance of characterisation techniques and basic reactor models during the development of new processes is emphasised.

**Keywords:** Electrochemical engineering; electrolyte flow; pressure drop; turbulence promoter.

**Nomenclature**

| Symbol | Meaning | Units |
|---|---|---|
| $A$ | Electrode area | $cm^2$ |
| $A_e$ | Electrode area per unit electrode volume | $cm^{-1}$ |
| $A_x$ | Cross-sectional area of flow channel | $cm^2$ |
| $B$ | Electrode breadth | cm |
| $d_e$ | Equivalent (hydraulic) diameter of channel (= $2BS/B+S$) | cm |
| $e$, $h$ | Empirical constants in equation (4) | dimensionless |
| $F$ | Faraday constant | C $mol^{-1}$ |
| $H$ | Electrode height | cm |
| $I_L$ | Limiting current | mA |
| $k_m$ | Space averaged mass transport coefficient | cm $s^{-1}$ |
| $\Delta p$ | Pressure drop | Pa |
| $P_{pump}$ | Power required for pumping | W |
| $Q$ | Volumetric flow rate of electrolyte | $cm^3$ $s^{-1}$ |
| $s_n$ | Normalised space velocity | $cm^3$ $cm^{-3}$ $s^{-1}$ |
| $S$ | Height of flow channel | cm |
| $t$ | Time | s |
| $v$ | Mean linear velocity of electrolyte | cm $s^{-1}$ |
| $V_R$ | Volume of cell (reactor) | $cm^3$ |
| $V_T$ | Volume of tank | $cm^3$ |
| $z$ | Electron stoichiometry | dimensionless |

*Greek*

| | | |
|---|---|---|
| $\varepsilon$ | Volumetric porosity of turbulence promoter | dimensionless |
| $\phi_{pump}$ | Pump efficiency | dimensionless |
| $\nu$ | Kinematic viscosity | $cm^2$ $s^{-1}$ |
| $\mu$ | Dynamic viscosity | g $cm^{-1}$ $s^{-1}$ |
| $\tau_R$ | Mean residence time in the cell (reactor) (= $V_R/Q$) | s |
| $\tau_T$ | Mean residence time in the tank (= $V_T/Q$) | s |

*Dimensionless groups*

| | | |
|---|---|---|
| $B/H$ | Working electrode breadth to height aspect ratio | dimensionless |
| $L/H$ | Working electrode length to height aspect ratio | dimensionless |
| $\gamma$ | Mass transport enhancement factor due to the TP | dimensionless |
| $Re$ | Channel Reynolds number (= $vd_e/\nu$) | dimensionless |
| $Sc$ | Schmidt number (= $\nu/D$) | dimensionless |
| $Sh$ | Sherwood number (= $k_m d_e/D$) | dimensionless |

**Abbreviations**

| | |
|---|---|
| CFL | C-Flow Lab 5 × 5 cell |
| TP | Turbulence promoter |
| LSV | Linear sweep voltammetry |
| NSV | Normalised space velocity |
| PFR | Plug flow reactor |
| 2D, 3D | Two-dimensional, three-dimensional |

## 1. Introduction

Electrochemical flow reactors are central to many electrochemical processes including organic electrosynthesis [1, 2], redox flow batteries [3, 4], and some types of water treatment [5]. Their importance in electrochemical technology has been highlighted recently [6]. Considerable attention has been given to the design and improvement of cell geometries, electrode materials and cell manufacture at different scales. This has sought to achieve an improved reaction environment with a more uniform distribution of current density and electrode potential, higher rates of mass transport to, or from, the electrode surface and lower capital and running costs [7].

The diversity of electrodes and applications in well-established rectangular channel laboratory cells has been the subject of extensive reviews. For instance, the FM01-LC reactor (originally developed by ICI C & P) has been fully characterised and its applications discussed by Rivera et al. [8, 9]. Developments beyond classical approaches can be found in the form of innovative manufacturing technology for flow frames, endplates, porous electrodes and turbulence promoters (TPs) using additive manufacturing [10]; the use of nanostructured porous electrodes [11]; and the coupling of electrode processes with heterogeneous reactions [5].

As pointed out in a critique of recent developments in rectangular channel flow cells [10], insufficient attention has been given to characterising the reaction environment of new cells; particularly those offered as ready solutions for laboratory studies. For example, some are intended for benchmarking of reactions in organic electrosynthesis [12, 13], the study of novel chemistries for flow batteries [14, 15] or multiple applications [16]. Such flow cells can actually be used for the development of entirely different electrochemical technologies. Nevertheless, we are not aware of any publication characterising the reaction environment in these, or similar new cells, for which pressure drop and average mass transport coefficients as

a function of flow rate are measured. These are essential parameters. Without such information, comparison and translation of results among different cells becomes difficult. Studies in this field need to use a well-defined experimental arrangement and a good understanding of the practical considerations regarding flow, limiting current and pressure drop, especially when attempting or describing new electrochemical processes.

This work provides a facile, basic characterisation of the hydrodynamic behaviour and electrochemical mass transport performance of the C-Flow® Lab 5 × 5 laboratory-scale electrochemical flow cell; commercialised by C-Tech Innovation Ltd. Planar electrodes were used for convenience and the effect of a TP in the flow channel was also investigated. The hydraulic flow pattern of a fluid through the channel, pressure drop over the reactor and space averaged mass transport to the electrode were examined at mean linear velocities in the range $2 < v < 10$ cm $s^{-1}$. The cell, which has typical dimensions used in laboratory studies, can accommodate a wide range of coated and uncoated electrode materials (planar and porous), and can be used in undivided or divided mode (with an ion exchange membrane or microporous separator between the two half-cells). Complete characterisation of the cell will allow us to understand better the effect of process parameters on diverse electrochemical reactions such as the anodic oxidation of ammonia coupled with hydrogen evolution at planar coated electrodes.

Standardised test cells, offer various advantages and limitations at different cost and availability. Additional practical aspects of laboratory cells and their expected features include: low contact electrical resistance, a small number of components, ease and speed of assembly, leakproof operation, freedom from blockage, ease of cleaning, ability to incorporate Luggin probes and other sensors, etc. From this perspective, it is imperative that characterisation of cell performances is made available, enabling users to make informed decisions.

## 2. Experimental details

### *2.1 The flow cell*

The studied cell has an active, projected electrode area, $A$ = 25 $cm^2$ and a half-cell working volume of 12.5 $cm^3$ (with a total of 25 $cm^3$ in the undivided mode), which is typical in laboratory studies. The configuration and cell components are shown in Figure 1. Brass current collectors, planar electrodes, gaskets, machined cPVC flow frames, flow distributors, and membrane gaskets were compressed between two stainless steel endplates. The two half-cells were separated by a proton exchange membrane Nafion 212 (Chemours Co.) having a dry thickness of 0.05 mm. The dimensions of the flow channel and working electrode, for the present rectangular channel cell, in comparison to other types of electrochemical cells are shown in Table 1. The flow frames of the studied cell have an overall dimension of 16 cm × 11 cm, both front and rear plate frames having a thickness of 0.7 cm. The flow channel has a length of 5 cm and a breadth of 5 cm.

As shown in Figure 1, both the front and rear plate frames have an inlet and an outlet manifold, each of them containing 6 consecutive ports of identical cross-sectional area (6.25 $mm^2$). Each port is at 90 deg to the axis of its respective manifold feeder. Electrolyte flow enters the compartment from the bottom inlet manifold, branches into separate streams through the ports, flows through the electrode compartment and travels towards the top outlet manifold. The front and rear plate frames also have two machined inserts each, with flow distributor patters facing the consecutive ports.

A 1.6 mm thick nickel (99.0%, Goodfellow UK Ltd.) and a 1.6 mm thick pure carbon sheet (C-Tech Innovation Ltd.) were used for the working and counter electrodes, respectively. The electrodes were 5 cm × 5 cm to give an active surface area of 25 $cm^2$. A chlorinated polyvinyl chloride (cPVC) mesh (supplied by C-Tech Innovation Ltd.) was mounted as a TP next to the planar electrode. The TP had overall dimensions of 6 cm × 6 cm × 0.1 cm and a volumetric

porosity, $\varepsilon$ , of 0.84. The value of $\varepsilon$ was determined from the ratio of the weight of the mesh to the weight of a solid piece of cPVC of the same overall dimensions, by the knowledge of its density. The structure of the mesh is shown in Figure 2 and was characterised using a Leo 1530 VP (Carl Zeiss A.G.) field emission gun scanning electron microscope.

*2.2 Flowing electrolytes*

An alkaline, aqueous electrolyte with the hexacyanoferrate(II)/hexacyanoferrate(III), redox couple was used for measurements of limiting current density and it was also used for the pressure drop measurements. The solution had a composition of $1.0 \times 10^{-3}$ mol $dm^{-3}$ $K_3[Fe(CN)_6]$ and $10.0 \times 10^{-3}$ mol $dm^{-3}$ $K_4[Fe(CN)_6]$ in 1.0 mol $dm^{-3}$ $Na_2CO_3$ (pH = 12.1). The excess of hexacyanoferrate(II) was used to ensure that the anodic reaction did not become rate limiting at the working electrode. The solution had a fluid density, $\rho$, of 1.12 g $cm^{-3}$; a dynamic viscosity, $\mu$, of $1.92 \times 10^{-2}$ g $cm^{-1}$ $s^{-1}$; and a kinematic viscosity, $\nu$ of $1.71 \times 10^{-2}$ $cm^2$ $s^{-1}$. The viscosity of the solution was measured with a digital Rheometer (Bohlin Gemini 200) at 25 °C.

*2.3 Flow visualisation*

Flow visualisation studies were carried out in order to obtain a qualitative indication of the electrolyte flow dispersion as it passed through the cell. The colour intensity of the methylene blue dye changed as a function of the local flow velocity and direction, and was filmed using a 40 megapixel digital camera (Huawei P20 pro) mounted on a tripod. A volume of 1 $cm^3$ of dye solution was injected by syringe, with the pump off, at a point located approximately 1 cm before the cell inlet. The pump was then switched on to start the test, avoiding the influence of the injection speed on the flow patterns. The test was performed at a representative mean linear velocity of 6 cm $s^{-1}$ and photographic images were taken at intervals of 0.25 s. For this procedure, one face of the cell was replaced with a transparent polymethyl methacrylate (PMMA) plate to enable the observation of the flow patterns. Given the qualitative nature of

this flow visualization study and the smooth surface of PMMA, it was assumed that the roughness factor of the surface had no substantial effect on the flow patterns.

*2.4 Pressure drop measurements*

The hydraulic pressure drop of the evaluated flow cell was measured with, and without, a TP present in the flow channel. A 3D image showing the internal structure of the flow frame can be seen in Figure 3a. The experimental arrangement for pressure drop measurements within the flow channel is shown in Figure 3b. Two holes of 2 mm diameter were drilled through the frame where pressure taps were inserted. One tap was positioned 5 mm above the top of the electrode and the other was 5 mm below the bottom of the electrode. The pressure drop of the fluid was also measured outside the frame to investigate the effect of manifolds, as shown in Figure 3c. For this, two T-piece connectors (Cole-Parmer UK Ltd.) were symmetrically positioned 20 mm away from the inlet and outlet manifolds.

The pressure taps were connected to a Digitron 2023P digital manometer (RS Components UK Ltd.) via two PTFE tubes of 2.4 mm internal diameter (Cole-Parmer UK Ltd.). For both configurations, pressure drop measurements were recorded every 30 s for 10 min to obtain an average value. The temperature of the solution was 24 °C. During these procedures, each compartment of the flow cell was connected to a peristaltic pump (Cole-Parmer Masterflex L/S) fitted with silicone rubber tubes (Masterflex L/S C-Flex Ultra) and to a reservoir (Duran GL 45) using silicone tubing with an internal diameter of 6.4 mm.

*2.5 Electrochemical mass transport studies*

The electrochemical performance of the cell under a mass transport-controlled electrode reaction was quantified using the mass transport coefficient, $k_m$ obtained by measuring steady-

state limiting currents, $I_L$ as a function of mean linear velocity, ranging from 2 to 10 cm $s^{-1}$. The reaction of interest at the nickel working electrode was the reduction of hexacyanoferrate(III) ion to hexacyanoferrate(II) ion:

$$Fe(CN)_6^{3-} + e^- \rightleftarrows Fe(CN)_6^{4-} \qquad E° = 0.361 \text{ V } \textit{vs.} \text{ SHE} \qquad (1)$$

Limiting current measurements for the reduction of hexacyanoferrate(III) ion were obtained by linear sweep voltammetry (LSV) between the potential limits of + 1.0 V and – 1.5 V *vs.* a saturated calomel reference electrode (SCE) at a linear sweep rate of 10 mV $s^{-1}$ using a carbon plate as the counter electrode. The scans were performed using a VoltaLab PZ1050 potentiostat (Radiometer Ltd.). As shown in Figure 3c, the working electrode potential was measured at its lateral, middle point through a Luggin capillary inserted in the flow frame and connected to an external reservoir containing the reference electrode. Experiments were carried out at a temperature of 24°C.

## 3. Theory

### *3.1 Mean linear velocity and Re number*

In order to enable the comparison of electrochemical flow cells across different scales and to define a simple normalised electrolyte flow rate, the mean linear velocity, $v$, of electrolyte past the electrode surface is calculated from its volumetric flow rate, $Q$, using the expression:

$$v = \frac{Q}{A_x \varepsilon} \qquad (2)$$

where $A_x$ is the cross-sectional area and $\varepsilon$ is the porosity of the flow channel.

The fluid flow of the electrolyte can then be described using the channel Reynolds number, $Re$. It is usually considered that well-developed flow in a smooth channel is laminar for $Re$ < 2100 and turbulent for $Re$ > 4000. The Reynolds number for the flow channel was determined from the mean linear velocity, $v$, by:

$$Re = \frac{vL}{\nu} \tag{3}$$

where $L$ is the length of the channel and $\nu$ is the kinematic viscosity. The range of solution flow evaluated in this work involved volumetric flow rates from 0.3 to 1.5 $dm^3$ $min^{-1}$, corresponding to mean linear velocities of 2 to 10 cm $s^{-1}$ past the electrode surface and channel Reynolds numbers in the range 53-265.

*3.1 Definition of an empirical power law for pressure drop*

The hydraulic pressure drop, $\Delta p$, experienced by the electrolyte as it flows through the cell is caused by frictional losses and its value is determined by the difference in pressure between two points. The relationship between $\Delta p$ and the flow conditions for a particular flow cell, enabling methodologies for evaluating electrode materials and improving pumping efficiency, can be described by an empirical power law:

$$\Delta p = eRe^h \tag{4}$$

where the coefficient, $e$, and the $Re$ exponent, $h$, are empirical constants which characterise a particular electrode geometry and flow cell. The power required for pumping, $P_{pump}$ is

related to the pressure drop, $\Delta p$ across the cell at a given volumetric flow rate, $Q$, by the expression:

$$P_{pump} = \frac{\Delta pQ}{\phi_{pump}} t \quad (5)$$

where $\phi_{pump}$ is the pump efficiency and $t$ is time.

*3.2 Limiting current density and mass transport rates*

The steady-state limiting current is achieved at the electrode when the current for the electrochemical reaction passing through the cell is restricted by the diffusion rate of electroactive species to and from the electrode surface. For a smooth, planar electrode, the relationship between $k_m$ and $I_L$ is:

$$k_m = \frac{I_L}{AzFc} \quad (6)$$

where $z$ is the electron stoichiometry, $F$ is the Faraday constant and $c$ is the bulk concentration of the reactant.

*3.3 The effect of the turbulence promoter*

Promotion of mixing and increased local velocities within the channel by the presence of a polymer mesh TP gives rise to an increase in mass transport to a planar electrode, at a given flow velocity. A mass transport enhancement factor, $\gamma$, can be quantified for a planar electrode by the ratio of the limiting current in the presence of the TP to that in the empty channel:

$$\gamma = \frac{I_{L\,(TP)}}{I_L} \tag{7}$$

In this work, the ratio indicates how much the limiting current at the nickel cathode increased by the addition of the cPVC TP.

## 4. Results and Discussion

### *4.1 Flow visualisation*

Flow visualization can be performed by injecting a dye [17], a fluorescent ink [18] or tracer particles [19]; a thermal imaging technique [20] may also be used. Its purpose is to reveal flow patterns and local electrolyte velocities within the flow channel, permitting the identification of possible stagnant areas, direction-changing vortices or non-uniform flow distribution. Such features can result in heterogeneous concentration and current distributions at the electrode which can lead, in turn, to parasitic reactions (e.g. gas evolution), mass transport restrictions and passivation or corrosion of the electrode surface. These issues become more relevant at the pilot and industrial scales [21] but it is a useful exercise to understand these principles in small cells, particularly in new designs.

The results of flow visualisation studies in the unrestricted electrode compartment with manifolds and flow frames are shown in Figure 4 for a typical mean linear velocity of 6 cm $s^{-1}$. It can be seen that initially the dye flowed into the compartment through the left vertical ports. An asymmetrical flow was generated within 1.0 s and was dominant at this side of the compartment. The dye started to emerge through the middle ports when the time reached 1.25 s. After 2.0 s, the blue dye occupied the left side of the compartment predominantly but can be observed entering the compartment through the right ports opposite to the inlet manifold. It

took approximately 4 s for the blue dye to fill the whole compartment, suggesting a relatively high flow dispersion in the direction perpendicular to the mainstream.

The flow maldistribution prominent at the left-hand side of the compartment is attributable to the geometry of the consecutive manifolds. This structure, consisting of multiple ports vertical to the manifold axis, is used widely due to its simplicity but is prone to producing non-uniform flow distribution. Typically, lateral ports next to the inlet manifold have excess flow, while others at the opposite end of the inlet suffer from shortages of flow. Non-uniform flow distribution in electrochemical flow reactors will reduce cell performance and efficiency [22]. Parameters, including the area ratio (the ratio of the sum of areas of all ports to manifold area), space between each two consecutive ports, curvature radius at the junction between manifold and ports, have a significant influence on flow distribution along the manifolds and can be improved to reduce the maldistribution effect [23]. For instance, by modifying the diameter of the ports or the diameter of the feeding tube as a function of their distance from the inlet [24]. It must be noted that such flow maldistribution is much less significant when 3D porous electrodes with small pore size are present in the flow channel, such as carbon felt [25].

*4.2 Pressure drop measurements*

Pressure drop is related to the pumping power demand and is therefore relevant to the efficiency of an electrochemical reactor. Reactions of interest are usually studied at an early stage on the laboratory scale, since a major aim is to determine feasibility. Comparative studies can evaluate the suitability of electrode materials [26], targeting low pressure drop for a given operational current density. Moreover, there are practical concerns regarding pressure drop in small cells, for example, surpassing the pumping pressure capacity [27], which causes deviations from the

nominal flow rate or the proclivity of electrolyte leaks when the internal cell pressure is needlessly high.

The hydraulic pressure drop, as a function of mean linear velocity, is presented in the logarithmic-logarithmic plot in Figure 5a for the C-Flow Lab cell, considering both an unrestricted flow compartment with a planar electrode and with a TP next to the electrode. The impact of cell manifolds has also been established by measuring the hydraulic pressure drop outside the cell frame. As expected, $\Delta p$ increased as a function of the mean linear velocity. The use of the TP next to the planar electrode resulted in a higher pressure drop through the flow cell. This is the same typical behaviour observed in industrial devices, such as the ElectroSynCell® (projected area of 400 $cm^2$) [28], where the pressure drop produced by the TP was close to that produced by a coarse nickel foam electrode. For the measurement taken within the cell frame, the highest pressure drop was obtained in the presence of the TP (max. 0.94 kPa at a mean linear velocity of 10 cm $s^{-1}$). In the absence of the TP, the pressure drop obtained at a mean linear velocity of 10 cm $s^{-1}$ was reduced to 0.86 kPa.

The cell manifolds had a significant effect on hydraulic pressure losses through the cell. The highest pressure drop measured outside the cell frame (max. 8.16 kPa at 10 cm $s^{-1}$) was almost one order of magnitude higher than that measured within the cell frame (max 0.94 kPa at 10 cm $s^{-1}$). These observations suggest that the consecutive ports increased friction at the walls and resulted in high resistance to fluid flow with increased pressure losses. Frías-Ferrer et al. [21] considered that, in small-scale electrochemical flow reactors, the flow reaction environment (e.g. flow pattern distribution, mass transport coefficients and current distribution) was largely dependent on the cell manifold geometry, position and number, rather than the flow channel characteristics. They proposed a geometrical manifold parameter, $\psi$, providing a simple but valuable statement of the importance of cell manifold design such as thickness,

width, geometrical distribution of the open spaces, and the free area for the electrolyte entrance, which can result in significant entrance/exit effects on hydraulic pressure drops.

Pressure losses through the flow cell in the present study can be compared with those produced by other types of electrochemical flow reactors and TP, also plotted in Figure 5a. For example, Arenas et al. [27] reported modest pressure losses through a TP mesh next to a Pt/Ti planar electrode, even at relatively high mean linear velocities. The highest $\Delta p$ value observed was 1.03 kPa at a mean linear velocity of 17 cm $s^{-1}$. On the other hand, Griffiths et al. [29] have examined the mass transport and pressure drop characteristics of the FM01 reactor. They confirmed that the use of a TP improved mass transport coefficients, at the expense of moderately higher pumping costs.

Other studies have discussed the use of porous electrodes. For instance, Brown et al. and Trinidad et al. [30, 31] reported the hydrodynamic behaviour of the FM01-LC reactor when using 3D porous electrodes and TPs. It was evident that their benefits included a higher mass transport coefficient at the electrode, more uniform current distribution, and reduced entrance effects near the inlet manifold. Arenas et al. [27] compared the pressure losses over various porous electrodes (a mesh, a micromesh and a felt) through an in-house built electrochemical flow reactor. They reported that the felt electrode (with $\varepsilon$ of 0.80) yielded the highest $\Delta p$ values (up to 259.5 kPa at 12 cm $s^{-1}$), whilst the lowest $\Delta p$ value (max. 264.4 Pa at 8 cm $s^{-1}$) was observed at the mesh electrode (with an $\varepsilon$ value of 0.71).

Pressure losses inside flow compartments have been researched for many years [32]. However, much less attention has been given to the other causes of partial pressure drops in a flow reactor (e.g. distribution ducts, branches, connecting beams, sudden section expansion). Pawlowski et al. considered all significant partial pressure drops of fluid flow inside a reverse electrodialysis (RED) stack and reported that the partial pressure drops in the distribution duct and the

branches had a dominant contribution to the cause of a non-uniform distribution in the stack [33].

A logarithmic-logarithmic plot can be used to establish the relationship between the pressure losses and the flow channel, *Re*, in the form of an empirical power law [27, 34, 35], see Figure 5b. The Reynolds number was calculated from mean linear velocities based on Equation (3). Following the typical behaviour [36], $\Delta p$ is linearly proportional to the Reynolds number under these conditions. The Reynolds number in the present study was relatively low in the flow channel ($Re < 300$). The correlations for the rectangular channel flow cell can also be compared with those for various porous electrodes in an in-house electrochemical flow reactor by Arenas et al. [27] and by Colli et al. [36].

*4.3 Mass transport measurements by limiting current*

Electrolyte flow entails convective diffusion of the products and reactants involved in an electrode reaction. As the ovepotential is increased, the reaction rate falls subsequently under charge transfer, mixed and mass transport control regimes [37]. In the latter two cases, electrode potentials (along with cell voltage) and the overall reaction rate are determined by forced convection. A limiting current is developed under full mass transport control, being a function of $k_m$, as shown by Equation (6). In turn, the value of $k_m$ is proportional to the electrolyte flow rate and depends, in part, on the geometry of the flow cell. The idealised, maximum production rate of a cell can be found by determining $k_m$ *vs.* electrolyte flow rate relationships, for instance, by the limiting current technique [38]. Poor mass transport (insufficient flow) can result in low limiting currents, undesired overpotentials and parasitic reactions. As a result, mass transport can influence the selectivity of electrochemical reactions [39].

Hydrodynamic linear voltammetry was carried out to determine an electrochemical performance factor, i.e., $k_m$, and to evaluate the impact of the implementation of TPs. A logarithmic-logarithmic plot, shown in Figure 6, is used to show the limiting current for reduction of ferricyanide ions in the flow cell as a function of the mean linear velocity in the absence and presence of the TP. The limiting current values increased from 4.5 to 20 mA as the mean linear velocity increased from 2 to 10 cm $s^{-1}$, which suggests enhanced convective-diffusion of electroactive species to and from the electrode surface in the flow channel. More importantly, the degree of enhancement in the limiting current was more pronounced when the TP was incorporated, contributing to an approximately four-fold increase in the limiting current at the lowest mean linear velocity studied (2 cm $s^{-1}$). Previous studies have reported that the deployment of an appropriate TP contributed to a significant increase in the mass transport coefficient [40], and also a more uniform distribution of mass transport over the electrode surface [41].

Figure 7 shows the mass transport coefficient in the electrode section as a function of the mean linear velocity in the absence and presence of the TP, according to Equation (6). The mass transport coefficient increased as the mean linear velocity increased. The incorporation of the TP enhanced the rate of mass transport to the electrode surface. Figure 8 shows the mass transport enhancement factor as a function of the mean linear rate. The employment of the TP showed an enhancement factor of up to 3.9 compared with the empty flow channel, which is marginally higher than those values reported by other researchers for different TPs, up to 2.2 [36] and 3.5 [42]. Similar mass transport enhancement effects take place at metal mesh electrodes [43]. The enhanced mass transport obtained in the present research is associated with the high volumetric porosity of the mesh promoter ($\varepsilon$ is 0.84). Incorporation of a mesh promoter in the fluid flow path significantly improved the rate of mass transport to the electrode

surface and hence its productivity over time. Furthermore, the TP can ameliorate the current and potential distribution at the electrode, reduce the effect of localised pH changes and decrease voltage efficiency losses [17].

It is noteworthy that the enhancement offered by the employment of the TP was more pronounced at a low mean linear rate and gradually decreased with increasing mean linear velocity. Previous studies have also reported this trend when assessing the mass transport enhancement factor of various electrode materials and they partly attributed this to the internal flow bypass (also called channelling) in the electrode compartment due to more intense manifold flow jets at higher mean linear velocities [44].

## 5. Predicted Cell Performance

### *5.1 Mass transport performance vs. pumping power*

Mass transport coefficients can be correlated to pressure drop, since both are functions of the mean electrolyte velocity. Such a plot considers the electrochemical performance of an electrode and/or cell in relation to the associated pressure drop over a range of flow rate, providing an indication of suitability for scale-up and permitting to establish empirical power laws that describe a particular cell design [27, 42]. Moreover, since pumping power is a function of pressure drop, this correlation gives an example of a simple cost-benefit approach which is useful for improving the technology readiness level of cells, and moving from the laboratory towards industrial processing.

The behaviour observed in the C-Flow Lab cell is shown in Figure 9. Given the similarities in their dimensions and type of TP, it is comparable to that of a 24 $cm^2$ electrode cell with planar Pt/Ti electrodes and a TP [27]. It can also be observed that the use of a TP results in both a higher mass transport coefficient and a higher pressure drop. This follows the expected

behaviour that cells with a high mass transport coefficient, tend to develop high pressure drop, due to the energy dissipation caused by the fluid mixing and turbulence taking place at the extended electrode surface area or at the TP structures. It is important to reach a practical compromise, such that the rate of mass transport to the electrode surface is sufficiently high at a moderate pressure drop over the cell.

*5.2 Predicted batch recirculation performance*

When the electrode reaction takes place at the highest possible current for a given mean linear velocity of electrolyte, i.e. the limiting current, it is possible to predict the fractional conversion of the reactant as a function of time by using the electrochemical plug flow reactor (PFR) model [45]. This also provides a means of illustrating the use of the mass transport coefficients determined previously in the description of the performance of the cell under the experimental conditions. A batch recirculation mode between the cell and an external electrolyte tank is considered [46].

Considering a $2e^-$ reduction under complete mass transport control in the batch recirculation flow mode via a 1 $dm^3$ catholyte tank, the time taken by the cell to achieve a fractional conversion of 90% for the reactant in a well-mixed tank is described by the PFR equation for batch recirculation [47]:

$$\log\left(\frac{c_{(t)}}{c_{(0)}}\right) = 2.3\frac{t}{\tau_T}\left[1 - \exp\left(\frac{k_m A}{Q}\right)\right] \quad (8)$$

and setting the ratio of reservoir concentration at time $t$, compared to the concentration at time zero, $c_{(t)}/c_{(0)}$ = 0.90, equivalent to an overall fractional conversion of 90%.

In equation (8), the symbols $A$, $k_m$, $\tau_T$, $c$ and $Q$ represent the electrode area, mass transport coefficient, mean residence time in the tank, reactant concentration and volumetric flow rate, respectively. The term in square parenthesis on the right-hand side of equation (8) represents the fractional reactant conversion in a single pass through the reactor while $t/\tau_T$ represents the number of recycles of electrolyte through the tank. The term in square brackets represents the fractional conversion of reactant in a single pass through the cell.

Considering a catholyte tank holding 1 $dm^3$ volume of electrolyte, the results are plotted as the time taken to achieve a fractional conversion of 90% in the tank, as a function of the mean flow velocity of electrolyte in Figure 10. The time was inversely proportional to the mean linear velocity and the application of the TP had a positive influence over the conversion rate. In the absence of the TP, the time decreased from 7 min to less than 2 min as the mean linear velocity increased from 2 to 10 cm $s^{-1}$. When the TP was incorporated, the time dropped significantly to 1.8 min at the lowest mean linear velocity and further reduced to 1 min as the mean linear velocity was increased to 10 cm $s^{-1}$.

*5.3 Normalised space velocity vs. mass transport performance*

The cell performance under the experimental conditions can be quantified and compared to other reactors by considering the normalised space velocity (NSV), $s_n$, ($dm^3$ $dm^{-3}$ $h^{-1}$) for 90% removal of a soluble contaminant for a mass transport-controlled reaction in the batch recirculation mode with a 1 $dm^3$ reservoir volume. The NSV can be calculated using the expression [48]:

$$s_n = \frac{k_m A}{2.3\, V_R} \tag{9}$$

where $A$ is the electrode area, $k_m$ is the mass transport coefficient, and $V_R$ is the reservoir volume. The NSV values for a fully mass transport-controlled reaction at various mean linear velocities, with and without a TP are shown in Figure 11. The values increased as a function of the mean linear velocity, since a higher rate of the electrolyte flow contributed to an increased mass transport coefficient. The employment of the TP further enhanced the mass transport in the flow channel and hence increased the NSV. The lowest value (0.073 $dm^3$ $dm^{-3}$ $h^{-1}$) was observed at the lowest mean linear velocity of 2 cm $s^{-1}$ without the TP. A mean linear velocity of 10 cm $s^{-1}$ in the presence of the TP yielded the highest NSV of 0.516 $dm^3$ $dm^{-3}$ $h^{-1}$.

These results can be contrasted with those at a planar carbon plate with a projected area of 19.2 $cm^2$ in a stirred beaker cell, which showed a NSV value of 0.49 $dm^3$ $dm^{-3}$ $h^{-1}$ for the recovery of Cu(II) ions at a constant current of 70 mA under a stirring rate of 1200 rpm [49]. At this scale, the productivity of the cell is not too different from that of a beaker cell with an electrode of comparable size. However, parallel plate flow cell has the advantage of a well-defined, controlled and reproducible reaction environment, in addition to the ability to scale up by increasing the volume of the tank [46].

## 6. Conclusions

The reaction environment in a laboratory rectangular channel flow cell using planar electrodes has been studied as a plug flow reactor, using a variety of techniques. The following conclusions can be drawn from the present studies:

1. Flow visualisation using methylene blue dye injection was conducted using a simple digital camera. An asymmetric flow was generated and dominant at one side of the compartment due to the geometry of multiple ports at 90 deg to the manifold axis.

2. The pressure drop increased as a function of the mean linear velocity and the channel Reynolds number. The values for the pressure losses obtained at a mean linear velocity of 10 cm $s^{-1}$ were increased from 0.86 kPa to 0.94 kPa as the TP was incorporated next to the planar nickel electrode. The cell manifolds had a significant influence on the hydraulic pressure drop through the flow channel. The highest pressure drop measured outside the cell frame (max. 8.16 kPa at 10 cm $s^{-1}$) was almost one order of magnitude higher than that measured within the cell frame (max 0.94 kPa at 10 cm $s^{-1}$).

3. The electrochemical performance of the flow cell was quantified from the limiting current and mass transport coefficient measurements. As mean linear velocities increased from 2 to 10 cm $s^{-1}$, the values for the limiting current were increased from 4.5 to 20 mA while the mass transport coefficient increased from 1.87 to 8.31 $10^{-3}$ cm $s^{1}$. At all flow velocities studied, the incorporation of a TP further enhanced the mass transport in the flow channel. The enhancement factor was between 1.6 and 3.9 at mean linear velocities in the range $2 < v < 10$ cm $s^{-1}$.

4. The implications of the data have been illustrated by plotting mass transport coefficient ($k_m$) *vs.* pressure drop in the electrode section of the channel over a range of mean electrolyte flow velocities. The correlation was typical for a flow-through cell using a 2D electrode and a TP. The plot of mass transport *vs.* pressure drop considers an aspect of electrochemical performance under mass transport control as a function of pumping power, useful for an informed scale-up of electrode materials, TP meshes, and cell designs.

5. The cell performance under the experimental conditions has been illustrated by calculating the time required to recirculate a fixed batch of electrolyte through the cell at controlled flow velocities in order to achieve a fractional reactant conversion of 90%, the reaction being completely mass transport controlled. In the absence of the TP, the time was decreased from 7 min to less than 2 min as the mean linear velocity increased from 2 to 10 cm $s^{-1}$. When the TP was incorporated, the time was significantly decreased to 1.8 min at the lowest mean linear velocity of 2 cm $s^{-1}$ and further reduced to 1 min as the mean linear velocity increased to 10 cm $s^{-1}$.

6. The cell performance under the experimental conditions has also been illustrated by considering the normalised space velocity ($dm^3$ $dm^{-3}$ $h^{-1}$) for 90% removal of a soluble contaminant via a mass transport-controlled reaction in the batch recycle mode with a 1 $dm^3$ reservoir volume. In the absence of the TP, the NSV values increased from 0.073 to 0.324 $dm^3$ $dm^{-3}$ $h^{-1}$ with increasing the mean linear velocity from 2 to 10 cm $s^{-1}$. Incorporation of the TP further increased the NSV values from 0.284 to 0.516 $dm^3$ $dm^{-3}$ $h^{-1}$.

Further studies will consider the pressure drop and electrochemical performance of the CFL cell in the presence of 3D, porous electrodes, such as metal mesh, metal foams, reticulated vitreous carbon and carbon felt.

## Acknowledgments

The authors from Coventry University would like to acknowledge Innovate UK and EPSRC for funding through the Energy Catalyst 4 Call under grant agreement No. EP/P03070X/1 and the Engineering Workshop at Coventry University for manufacturing transparent cell components.

## References


[1] A. Wiebe, T. Gieshoff, S. Möhle, E. Rodrigo, M. Zirbes, S. R. Waldvogel, *Angew Chem Int Ed.*, **57**, 5594 (2018).

[2] M. Atobe, H. Tateno, Y. Matsumura, *Chem Rev.*, **118**, 4541 (2017).

[3] X. Wei, W. Pan, W. Duan, A Holla, Y. Zhang, Z. Yang, B. Li, Z. Nie, J. Liu, D. Reed, W. Wang, V. Sprenkle, *ACS Energy Lett.*, **2**, 2187 (2017).

[4] M. H. Chakrabarti, E. P. L. Roberts, C. Bae, M. Saleem, *Energy Convers. Manage.*, **52**, 2501 (2011).

[5] F. C. Moreira, R. A. R. Boaventura, E. Brillas, V. J. P. Vilar, *App Catal B: Environ.*, **202**, 217 (2017).

[6] K. Scott, *Renew Sust Energ Rev.*, **81**, 1406 (2018).

[7] S. Bebelis, K. Bouzek, A. Cornell, G. H. Kelsall, M. G. S. Ferreira, F. Lapicque, C. Ponce de León, M. A. Rodrigo, F. C. Walsh, *Chem. Eng. Res. Des.*, **91**, 1998 (2013).

[8] F. F. Rivera, C. Ponce de León, F. C. Walsh, J. L. Nava, *Electrochim. Acta*, **163**, 338 (2015).

[9] F. F. Rivera, C. Ponce de León, F. C. Walsh, J. L. Nava, *Electrochim. Acta*, **161**, 436 (2015).

[10] F. C. Walsh, L. F. Arenas, C. Ponce de León, *Curr. Opin. Electrochem.*, **16**, 10 (2019).

[11] M. J. Kim, M. A. Cruz, F. Yang, B. J. Wiley, *Curr. Opin. Electrochem.*, **16**, 19 (2019).

[12] C. Gütz, A. Stenglein, S. R. Waldvogel, *Org. Process Res. Dev.*, **21**, 771 (2017).

[13] R. A. Green, R. C. D. Brown, D. Pletcher, B. Harji, *Org. Process Res. Dev.*, **19**, 1424 (2015).

[14] C-Flow 5×5 Electrochemical Cell Brochure. C-Tech Innovation Ltd., 2019. https://www.ctechinnovation.com/product/c-flow-5x5/

[15] Flow Battery Lab-Cell. Pinflow energy Storage, S.R.O., 2019. http://pinflowes.com/assets/img/ProductsResearch/LabCellTechSpec.pdf

[16] Micro Flow Cell Technical Data. ElectroCell A/S., 2019. https://www.electrocell.com/media/1215/micro-flow-cell_technical-data.pdf

[17] L. Castañeda, R. Antaño, F. F. Rivera, J. L. Nava, *Int. J Electrochem. Sci.*, **12**, 7351 (2017).

[18] A. A. Wong, M. J. Aziz, S. Rubinstein, *ECS Trans.* **77**(11), 153 (2017).

[19] G. Rodríguez, F. Z. Sierra-Espinosa, A. Álvarez, F. Carrillo, *Desalin. Water Treat.*, **73**, 127 (2017).

[20] H. Tanaka, Y. Miyafuji, J. Fukushima, T. Tayama, T. Sugita, M. Takezawa, T. Muta, *J Energy Storage*, **19**, 67 (2018).

[21] A. Frías-Ferrer, J. González-García, V. Sáez, C. Ponce de León, F. C. Walsh, *AIChE J.*, **54**, 811 (2008).

[22] J. Wang, *Chem. Eng. J.*, **168**, 1331 (2011).

[23] J. M. Hassan, A. AbdulRazzaq, B. K. Kamil, *J. Eng. and Dev.*, **12**, 159 (2008).

[24] J. M. Hassan, T. A. Mohamed, W. S. Mohammed, W. H. Alawee, *J. Fluids*, 325259 (2014).

[25] J. González-García, P. Bonete, E. Expósito, V. Montiel, A. Aldaz, R. Torregrosa-Maciá, *J. Mater. Chem.*, **9**, 419 (1999).

[26] A. Forner-Cuenca, E. E. Penn, A. M. Oliveira, F. R. Brushett, *J. Electrochem. Soc.*, **166**, A2230 (2019).

[27] L. F. Arenas, C. Ponce de León, F. C. Walsh, *AIChE J.*, **64**, 1135 (2018).

[28] A. Montillet, J. Comiti, J. Legrand, *J Appl Electrochem.*, **23**, 1045 (1993).

[29] M. Griffiths, C. Ponce de Leon, F. C. Walsh, *AIChE J.*, **51**, 682 (2005).

[30] C. J. Brown, D. Pletcher, F. C. Walsh, J. K. Hammond, D. Robinson, *J. Appl. Electrochem.*, **24**, 95 (1994).

[31] P. Trinidad, F. C. Walsh, *Electrochim. Acta*, **41**, 493 (1996).

[32] A. Storck, D. Hutin, *Electrochim Acta*, **26**, 127 (1981).

[33] S. Pawlowski, J. G. Crespo, S. Velizarov, *J. Membr. Sci.*, **462**, 96 (2014).

[34] C. J. Brown, D. Pletcher, F. C. Walsh, J. K. Hammond, D. Robinson, *J. Appl. Electrochem.*, **23**, 38 (1993).

[35] T. R. Ralph, M. L. Hitchman, J. P. Millington, F. C. Walsh, *Electrochim. Acta*, **41**, 591 (1996).

[36] A. N. Colli, R. Toelzer, M. E. H. Bergmann, J. M. Bisang, *Electrochim. Acta*, **100**, 78 (2013).

[37] D. Pletcher, *A First Course in Electrode Processes*, 2nd Edn, The Royal Society of Chemistry (2009).

[38] P. Cañizares, J. García-Gómez, I. Fernández de Marcos, M. A. Rodrigo, J. Lobato, *J. Chem. Educ.*, **83**, 1204 (2006).

[39] P.-C. Cheng, T. Nokata, *J. Electroanal. Chem.*, **269**, 223 (1989).

[40] N. G. Carpenter, E. P. L. Roberts, *Trans IChemE*, **77**, 212 (1999).

[41] W. M. Taama, R. E. Plimley, K. Scott, *Electrochim Acta*, **41**, 543 (1996).

[42] C. J. Brown, F. C. Walsh, D. Pletcher, *Trans IChemE*, **73**, 196 (1995).

[43] F. Leroux, F. Coeuret, *Electrochim Acta*, **30**, 159 (1985).

[44] A. R. Da Costa, F. G. Fane, *Ind. Eng. Chem. Res.*, **33**, 1845 (1994).

[45] A. Walker, A. A. Wragg, *Electrochim. Acta*, **22**, 1129 (1977).

[46] D. Pletcher, R. A. Green, R. C. D. Brown, *Chem. Rev.*, **118**, 4573 (2017).

[47] F. C. Walsh, P. Trinidad, D. Gilroy, *Int. J. Engng. Ed.*, **21**, 981 (2005).

[48] G. Kreysa, *J. Appl. Electrochem.*, **15**, 175 (1985).

[49] G. A. Ottewill, G. W. Reade, S. A. Campbell, C. Ponce de León, F. C. Walsh, *J. Environ. Monit.*, **7**, 943 (2005).

# Tables

| Parameter for each half-cell in divided configuration. | This work, C-Flow Lab cell | Waldvogel cell* [12] | Pinflow Lab-Cell† [15] | ElectroCell Micro Flow Cell‡ [16] | Arenas et al. in-house cell [23] | Griffiths et al. FM01-LC cell [24] | Ralph et al. in-house cell [30] |
|---|---|---|---|---|---|---|---|
| Flow channel length, $L$ / cm | 5 | 6 | 5 | 3.2 | 6 | 16 | 15 |
| Flow channel breath, $B$ / cm | 5 | 2 | 4 | 3.2 | 4 | 4 | 15 |
| Flow channel height, $S$ / cm | 0.5 | 0.2 | 0.5 | 0.4 | 0.6 | 0.45 | 1.0 |
| Projected electrode area, $A$ / $cm^2$ | 25 | 12 | 20 | 10 | 24 | 64 | 225 |
| Channel volume, V / $cm^3$ | 12.5 | 2.4 | 10 | 4 | 14.4 | 28.8 | 225 |
| Hydraulic equivalent diameter, $d_e$ / cm (= $2BS$ / $B$+$S$) | 0.91 | 0.36 | 0.89 | 0.71 | 1.04 | 0.81 | 1.88 |
| W.E. breadth to height aspect ratio (= $B$/$S$) | 10 | 10 | 8 | 7.9 | 6.67 | 8.89 | 15 |
| W.E. length to height aspect ratio (=$L$/$S$) | 10 | 30 | 10 | 7.9 | 10 | 35.56 | 15 |
| Standard frame material | CPVC | PTFE | PVC | PTFE | PMMA | PTFE | PVC |

Table 1. Typical geometrical dimensions of the half-cell channel and working electrode for various laboratory flow cells. For comparison purposes, all cells are considered with a 2D, planar electrode. *Using the thickest recommended gasket of 2 mm. †For an electrode height option of 5 mm. ‡For a standard electrode gap of 4 mm. Cell architecture and dimensions by commercial suppliers differ depending on application or by request.

# Figure captions

**Fig. 1.** Expanded view showing the configuration of the CFL electrochemical cell. 1) rear plate assembly (304 stainless steel); 2) current collector (brass); 3) electrodes (nickel or carbon); 4) electrode gaskets (expanded EPDM); 5) flow frames (cPVC); 6) flow distributor inserts (cPVC); 7) membrane gaskets (EPDM); 8) membrane (Nafion 212); 9) front plate assembly (304 stainless steel); 10) compression thumb screws (304 stainless steel). Courtesy of C-Tech Innovation Ltd.

**Fig. 2.** SEM image showing the structure of the turbulence promoter (TP), an electrochemically inert cPVC mesh, along its average pitch dimensions.

**Fig. 3.** Electrochemical cell and experimental arrangement for pressure drop measurements. a) 3D images showing the internal structure of the flow distribution frame. Courtesy of C-Tech Innovation Ltd. b) Arrangement for measurements within the flow channel c) Arrangement for measurements outside the cell frame using T-piece connectors.

**Fig. 4.** Flow visualisation images of the flow channel, following the injection of methylene blue dye into the inlet, at time, $t = 0$ at a representative mean linear velocity of 6 cm $s^{-1}$. Image captured by a digital camera, at 0.25 s intervals until $t = 3.75$ s.

**Fig. 5.** Pressure drop experienced by the flowing electrolyte as it passes through the electrode compartment and whole electrochemical flow cell in the absence and presence of a TP. Pressure drop *vs.* a) electrolyte mean linear velocity, and b) Reynolds number. Electrolyte composition: $1.0 \times 10^{-3}$ mol $dm^{-3}$ $K_3[Fe(CN)_6]$ and $10.0 \times 10^{-3}$ mol $dm^{-3}$ $K_4[Fe(CN)_6]$ in 1.0 mol $dm^{-3}$ $Na_2CO_3$.

**Fig. 6.** Limiting current density measurements for reduction of ferricyanide ions at a planar cathode in a channel in the absence and presence of a TP mesh over a range of controlled mean linear velocity. Electrolyte composition: $1.0 \times 10^{-3}$ mol $dm^{-3}$ $K_3[Fe(CN)_6]$ and $10.0 \times 10^{-3}$ mol $dm^{-3}$ $K_4[Fe(CN)_6]$ in 1.0 mol $dm^{-3}$ $Na_2CO_3$. Linear sweep voltammetry (LSV) performed between the potential limits of + 1.0 V and – 1.5 V *vs.* SCE at a linear sweep rate of 10 mV $s^{-1}$ at 24°C. Mean linear velocities in the range $2 < v < 10$ cm $s^{-1}$.

**Fig. 7.** Mass transport coefficient measurements for reduction of ferricyanide ions at a planar cathode in a channel containing a TP mesh over a range of controlled mean linear velocity in the range $2 < v < 10$ cm $s^{-1}$. Electrolyte composition: $1.0 \times 10^{-3}$ mol $dm^{-3}$ $K_3[Fe(CN)_6]$ and $10.0 \times 10^{-3}$ mol $dm^{-3}$ $K_4[Fe(CN)_6]$ in 1.0 mol $dm^{-3}$ $Na_2CO_3$. Linear sweep voltammetry (LSV) performed between the potential limits of + 1.0 V and – 1.5 V *vs.* SCE at a linear sweep rate of 10 mV $s^{-1}$ and at 24°C.

**Fig. 8.** Mass transport enhancement factor to the planar nickel electrode due to the presence of a TP over a range of electrolyte mean linear velocity. Electrolyte composition: $1.0 \times 10^{-3}$ mol $dm^{-3}$ $K_3[Fe(CN)_6]$ and $10.0 \times 10^{-3}$ mol $dm^{-3}$ $K_4[Fe(CN)_6]$ in 1.0 mol $dm^{-3}$ $Na_2CO_3$. Temperature 24°C.

**Fig. 9.** Mass transport coefficient *vs.* pressure drop in the electrode section of the channel with mean electrolyte flow velocities in the range $2 < v < 10$ cm $s^{-1}$. Electrolyte composition: $1.0 \times 10^{-3}$ mol $dm^{-3}$ $K_3[Fe(CN)_6]$ and $10.0 \times 10^{-3}$ mol $dm^{-3}$ $K_4[Fe(CN)_6]$ in 1.0 mol $dm^{-3}$ $Na_2CO_3$. Temperature 24°C.

**Fig. 10.** Expected time taken to achieve a fractional conversion of 90% for an idealised two-electrode reaction as a function of mean linear velocity of electrolyte, according to Equation (8).

**Fig. 11.** Predicted values of normalised space velocity as a function of mean linear velocity for an idealized two-electrode reaction, in the absence and presence of a TP in the flow channel, according to Equation (9).

# Figures

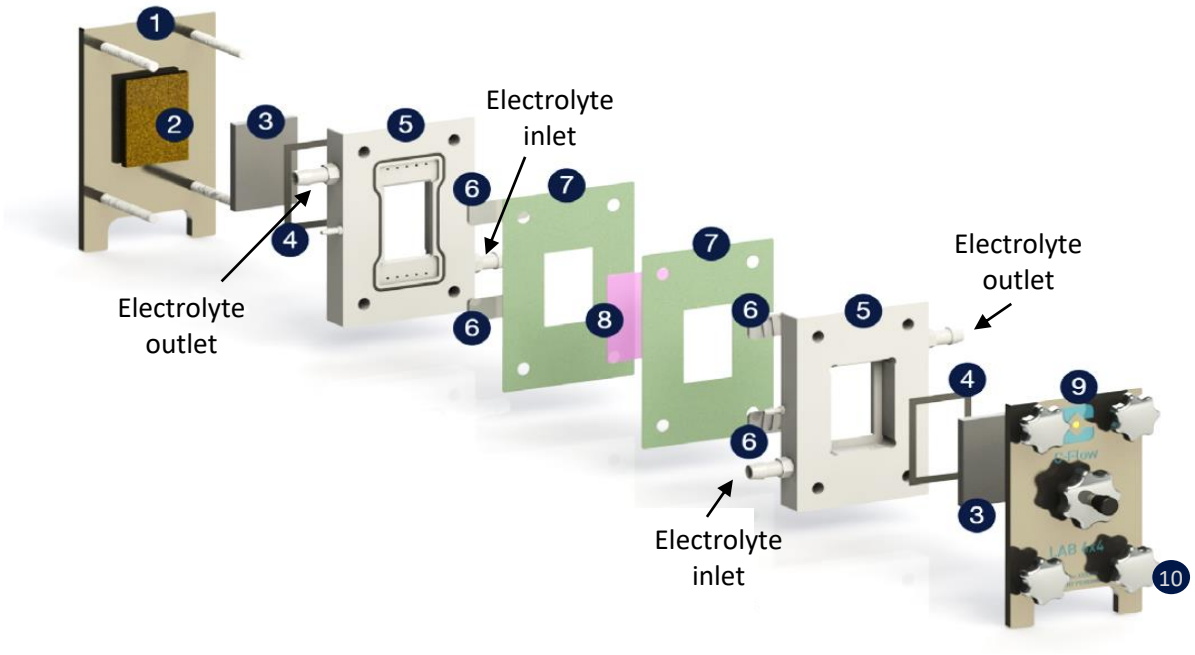


Fig. 1

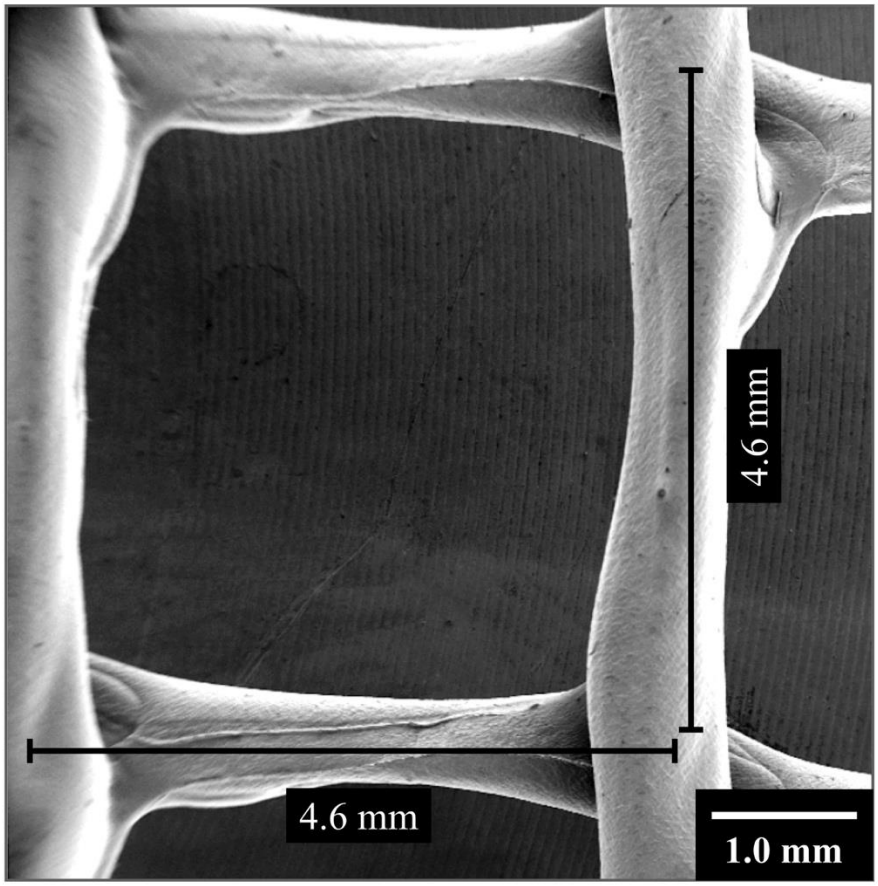


Fig. 2

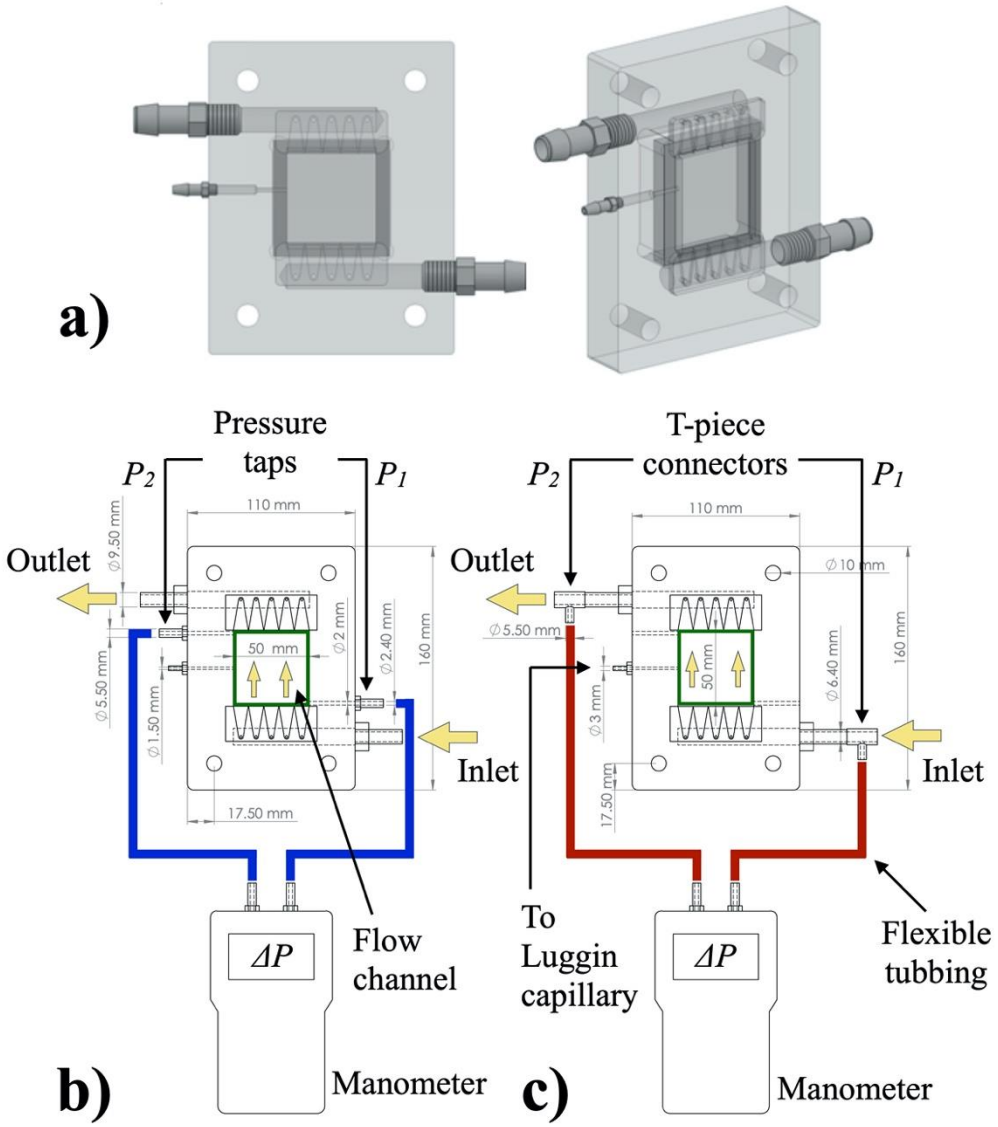
a)
Pressure
taps
$P_2$
$P_1$
110 mm
Outlet
Ø9.50 mm
Ø2 mm
Ø2.40 mm
160 mm
50 mm
Ø5.50 mm
Ø1.50 mm
Inlet
17.50 mm
ΔP
Flow
channel
Manometer
b)
T-piece
connectors
$P_2$
$P_1$
110 mm
Outlet
Ø10 mm
Ø5.50 mm
50 mm
Ø6.40 mm
160 mm
Ø3 mm
Inlet
17.50 mm
To
Luggin
capillary
ΔP
Flexible
tubbing
Manometer
c)

Fig. 3

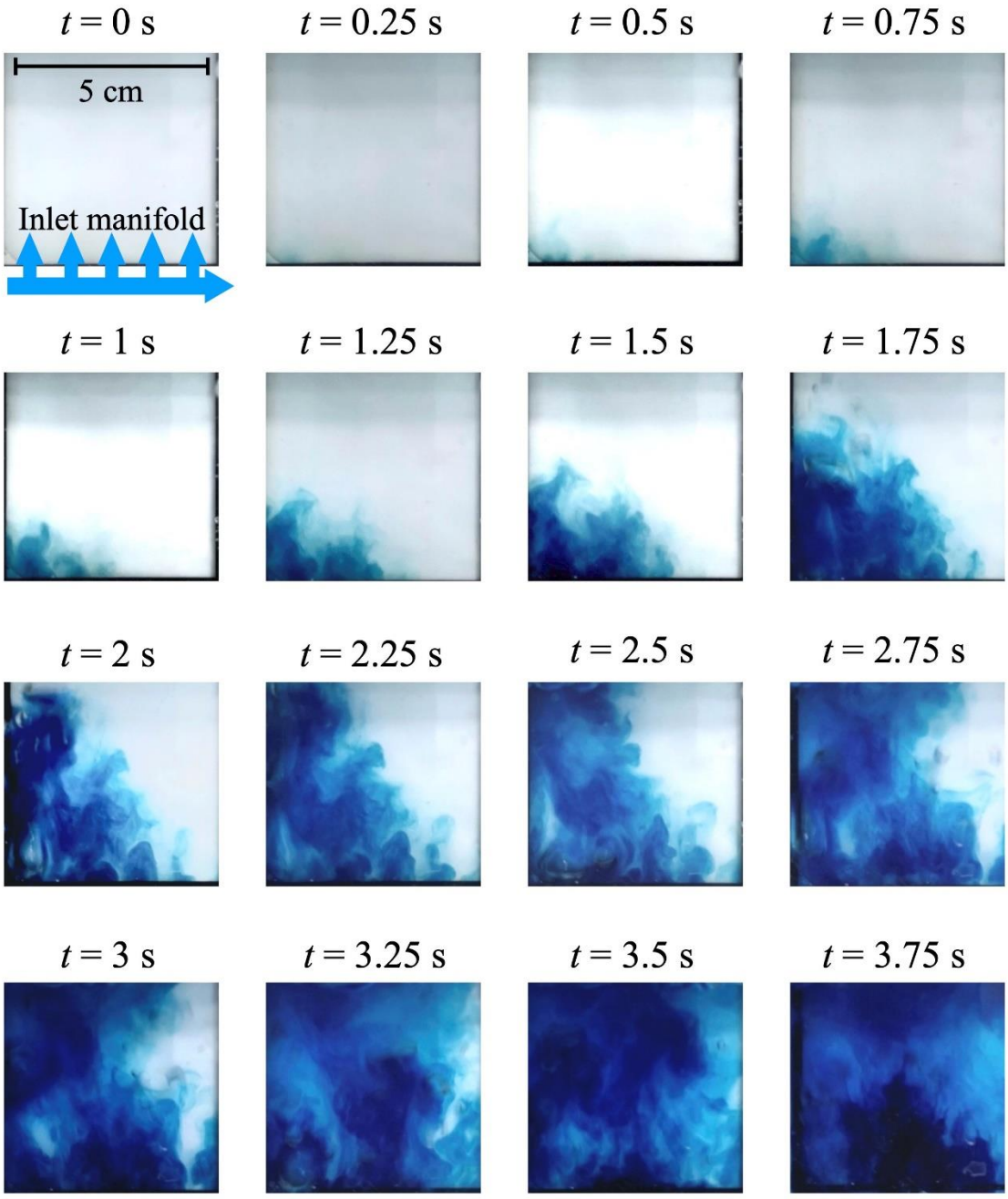
t = 0 s
5 cm
Inlet manifold
t = 0.25 s
t = 0.5 s
t = 0.75 s
t = 1 s
t = 1.25 s
t = 1.5 s
t = 1.75 s
t = 2 s
t = 2.25 s
t = 2.5 s
t = 2.75 s
t = 3 s
t = 3.25 s
t = 3.5 s
t = 3.75 s

Fig. 4

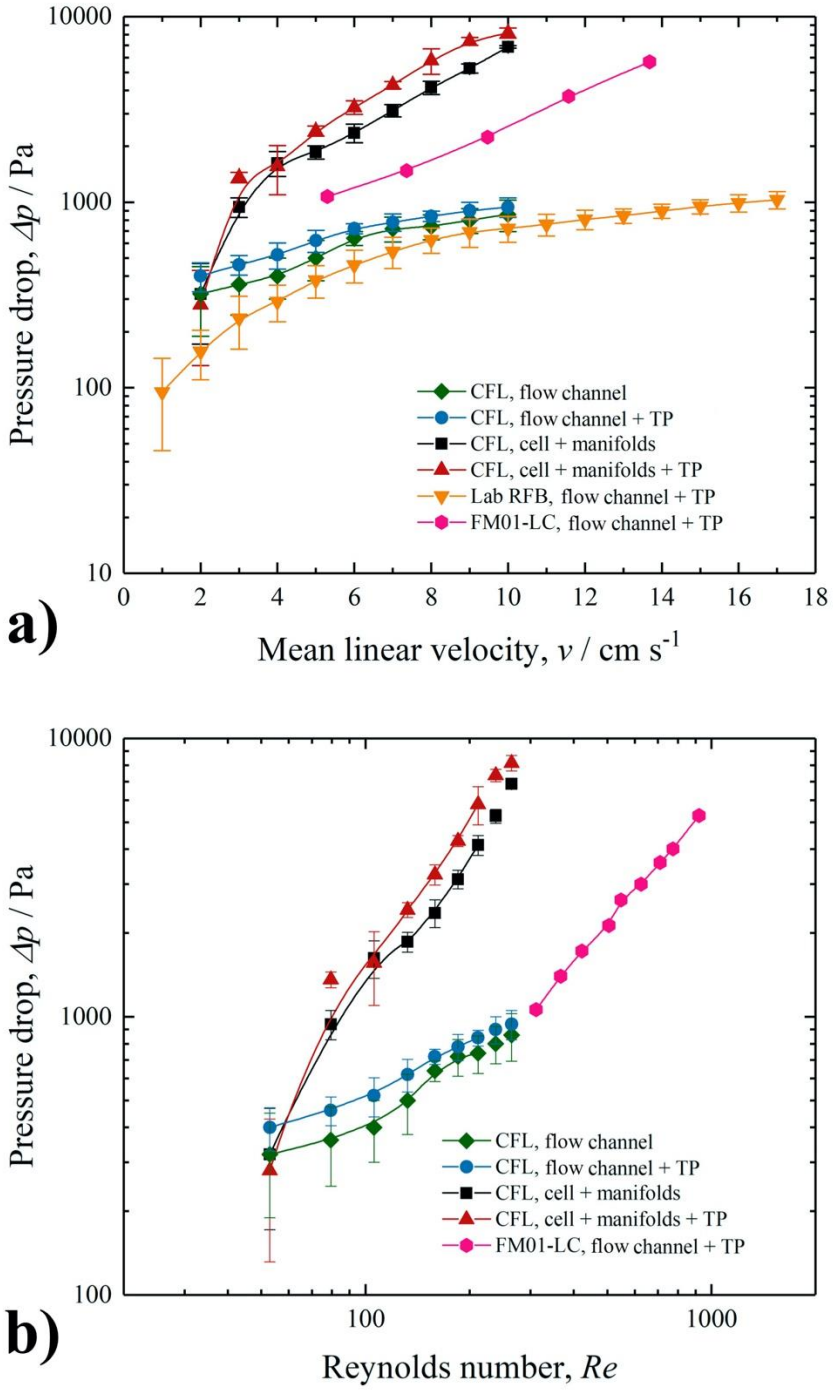
a)
Pressure drop, Δp / Pa
Mean linear velocity, v / cm s-1
CFL, flow channel
CFL, flow channel + TP
CFL, cell + manifolds
CFL, cell + manifolds + TP
Lab RFB, flow channel + TP
FM01-LC, flow channel + TP
b)
Pressure drop, Δp / Pa
Reynolds number, Re
CFL, flow channel
CFL, flow channel + TP
CFL, cell + manifolds
CFL, cell + manifolds + TP
FM01-LC, flow channel + TP

Fig 5.

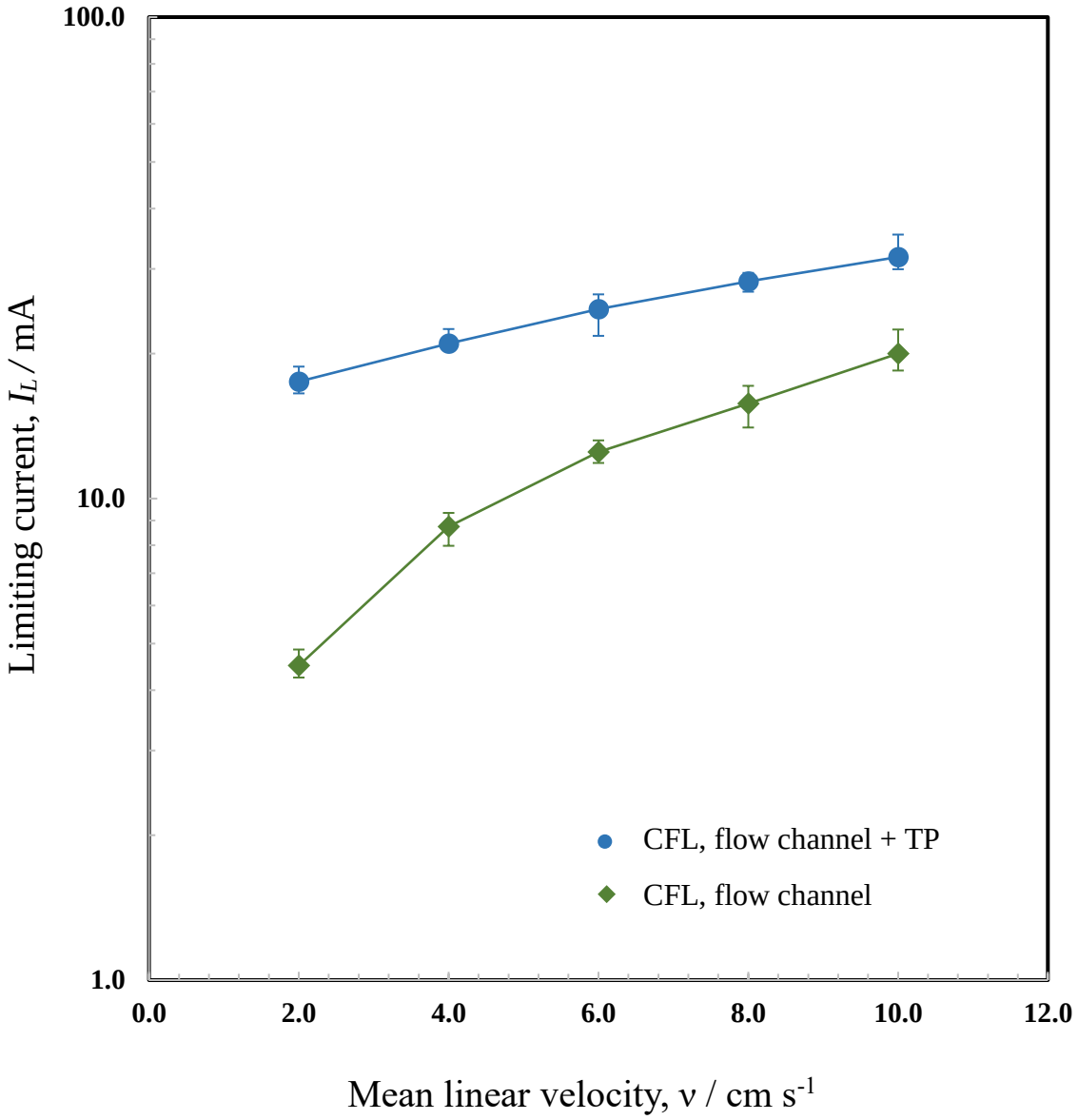
100.0
10.0
1.0
0.0
2.0
4.0
6.0
8.0
10.0
12.0
Limiting current, $I_L$ / mA
Mean linear velocity, ν / cm s$^{-1}$
CFL, flow channel + TP
CFL, flow channel

Fig. 6

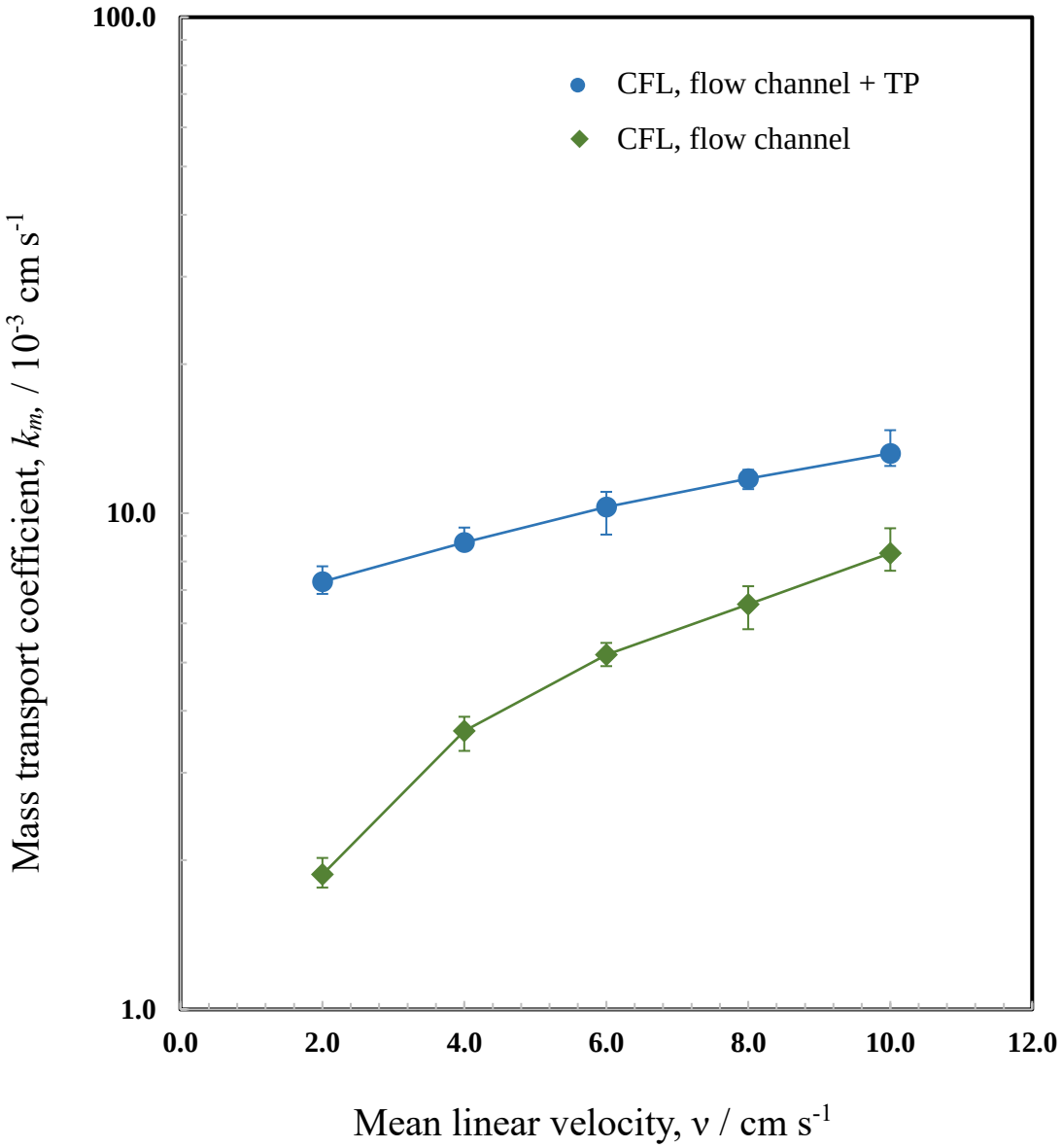
100.0
10.0
1.0
0.0
2.0
4.0
6.0
8.0
10.0
12.0
CFL, flow channel + TP
CFL, flow channel
Mass transport coefficient, $k_m$, / $10^{-3}$ cm $s^{-1}$
Mean linear velocity, v / cm $s^{-1}$

Fig. 7

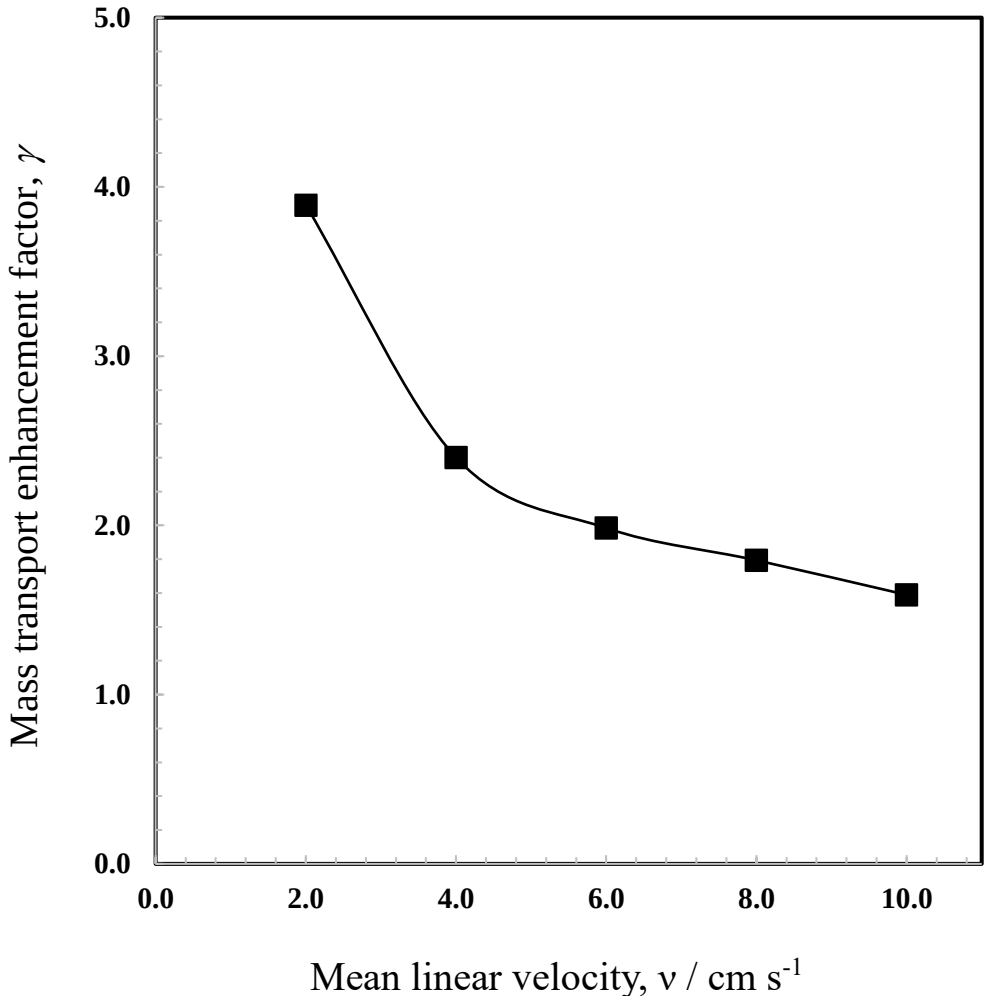
Mass transport enhancement factor, γ
5.0
4.0
3.0
2.0
1.0
0.0
0.0
2.0
4.0
6.0
8.0
10.0
Mean linear velocity, ν / cm s-1

Fig. 8

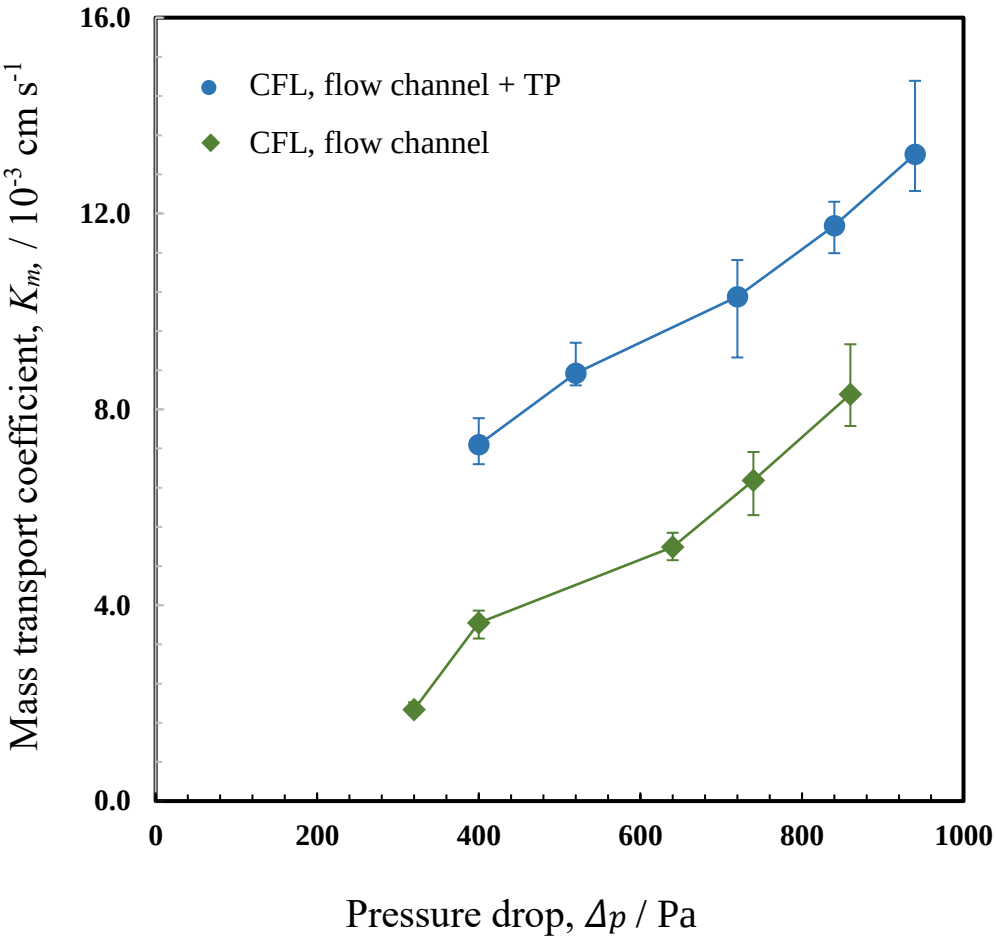
16.0
12.0
8.0
4.0
0.0
0
200
400
600
800
1000
CFL, flow channel + TP
CFL, flow channel
Mass transport coefficient, $K_m$, / $10^{-3}$ cm $s^{-1}$
Pressure drop, $\Delta p$ / Pa

Fig. 9

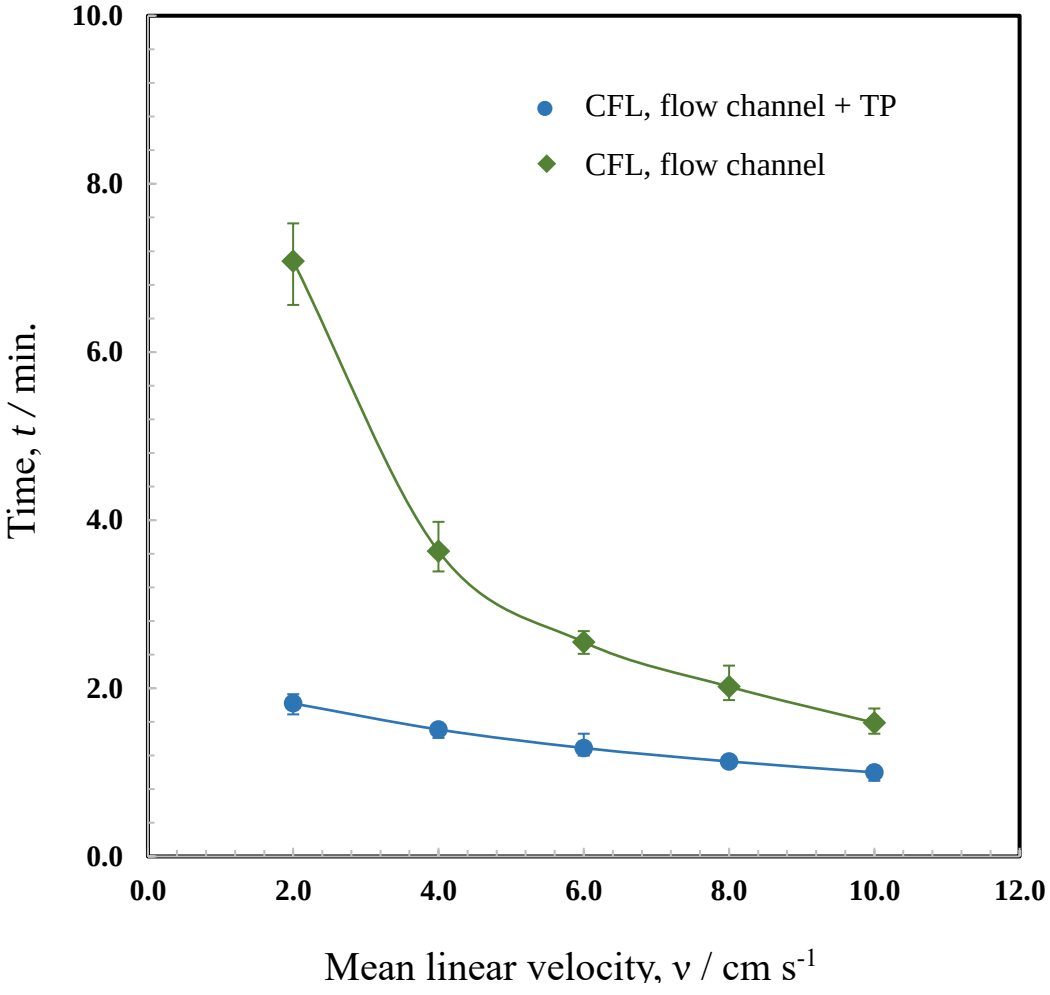
10.0
8.0
6.0
4.0
2.0
0.0
Time, t / min.
CFL, flow channel + TP
CFL, flow channel
0.0
2.0
4.0
6.0
8.0
10.0
12.0
Mean linear velocity, ν / cm s-1

Fig. 10

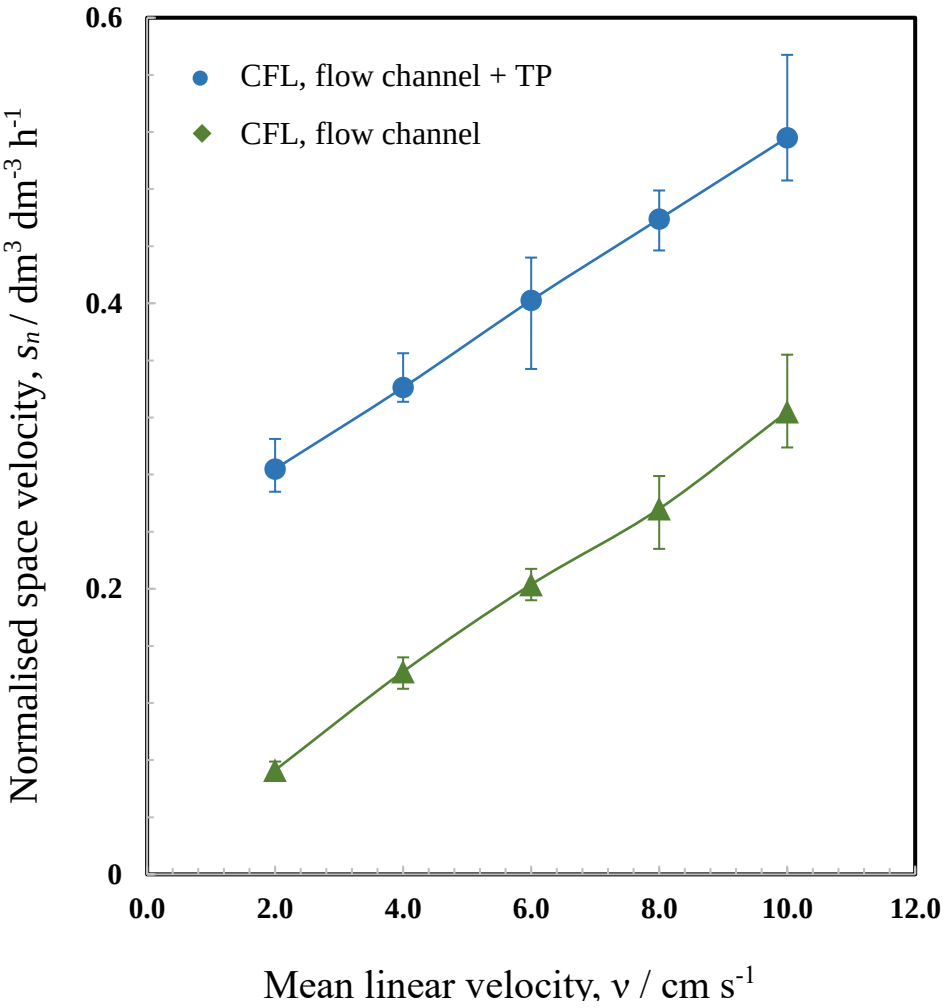
0.6
0.4
0.2
0
0.0
2.0
4.0
6.0
8.0
10.0
12.0
CFL, flow channel + TP
CFL, flow channel
Normalised space velocity, $s_n$ / dm$^3$ dm$^{-3}$ h$^{-1}$
Mean linear velocity, v / cm s$^{-1}$

Fig. 11